PCCP

PAPER

View Article Online
View Journal | View Issue

Cite this: *Phys. Chem. Chem. Phys.*, 2014, **16**, 17018

A quantum chemical study on gas phase decomposition pathways of triethylgallane (TEG, $Ga(C_2H_5)_3$) and *tert*-butylphosphine (TBP, $PH_2(t\text{-}C_4H_9)$) under MOVPE conditions†

Andreas Stegmüller, Phil Rosenow and Ralf Tonner*

Received 11th April 2014,
Accepted 24th June 2014

DOI: 10.1039/c4cp01584c

www.rsc.org/pccp

The gas phase decomposition reactions of precursor molecules relevant for metal–organic vapour phase epitaxy (MOVPE) of semiconductor thin films are investigated by computational methods on the density-functional level as well as on the *ab initio* (MP2, CCSD(T)) level. A comprehensive reaction catalogue of uni- and bimolecular reactions is presented for triethylgallium (TEG) as well as for *tert*-butylphosphine (TBP) containing thermodynamic data together with transition state energies. From these energies it can be concluded that TEG is decomposed in the gas phase under MOVPE conditions (T = 400–675 °C, p = 0.05 atm) to GaH_3 *via* a series of β-hydride elimination reactions. For elevated temperatures, further decomposition to GaH is thermodynamically accessible. In the case of TBP, the original precursor molecule will be most abundant since all reaction channels exhibit either large barriers or unfavorable thermodynamics. Dispersion-corrected density functional calculations (PBE-D3) provide an accurate description of the reactions investigated in comparison to high level CCSD(T) calculations serving as benchmark values.

1. Introduction

Semiconductor materials composed of group 13 and group 15 elements (aka. III/V materials) grown on silicon surfaces have potential applications as highly efficient solar cells and lasers.[1] "Silicon photonics" aims at the combination of optical data processes with Si-based microelectronics technology, but is hampered by the indirect band gap of silicon and thus optically active overlayers have to be formed.[2] These materials are often deposited onto silicon substrates by a vapor phase epitaxy procedure from metal–organic precursor molecules (MOVPE). In order to tune the materials towards direct optical gaps, metastable quaternary group III/V materials were developed which exhibit lattice constants close to the Si bulk value.[3] However, these materials can be grown quasi-epitaxially on Si(001) applying a 40–50 nm buffer layer of GaP.[4,5] The quality of the III/V material's optoelectronic properties is highly dependent on the structural quality of the GaP nucleation layer which goes hand in hand with the cleanliness of the Si substrate surface, choice and purity of the precursors and the specific suitability of the applied growth conditions.[6] Crystal defects can be propagated by mechanical strain caused by the heterolayers' lattice mismatch to silicon or different thermal expansion coefficients. On the other hand, non-ideal reactor conditions lead to incomplete precursor decomposition and undesirable doping defects, *e.g.* carbon incorporation.[7] It is the declared goal of material scientists to minimize these defects during growth of promising III/V materials. Therefore, a detailed understanding of the chemical processes within the reactor is crucial and computational studies are used to complement experimental findings.[9–12] It is, for instance, difficult to obtain reaction-specific barriers from experiment (*e.g.* mass spectrometry) as the appearance of detected species can only be related to the overall temperature and reaction (growth) rate.[8,12,16]

One frequently applied precursor in the growth of III/V materials is trimethylgallane ($Ga(CH_3)_3$, TMG), which has a lower decomposition rate than triethylgallane ($Ga(C_2H_5)_3$, TEG) and pyrolyzes only at high temperatures (above 480 °C)[16] in the gas phase. Surface-assisted decomposition mechanisms, on the other hand, exhibit significantly lower barriers (<130 °C).[14] However, there is an increased tendency for carbon incorporation, because reactive and therefore uncontrollable radical species are formed from TMG, *e.g.* dimethylgallane and methyl radicals, which remain strongly bound to the Si surface.[12,14] By introducing ligands larger than methyl, decomposition temperatures (thermal barriers) were found to decrease: tri-*tert*-butylgallane, *e.g.*, undergoes clean decomposition *via* β-hydride elimination already at 260 °C (low barrier of 160 kJ mol^{-1})[15]

Fachbereich Chemie and Materials Sciences Center, Philipps-Universität Marburg, Hans-Meerwein-Strasse, 35032 Marburg, Germany.
E-mail: tonner@chemie.uni-marburg.de

† Electronic supplementary information (ESI) available. See DOI: 10.1039/c4cp01584c

without carbon incorporation.[16] It has been found that this problem can be circumvented by using TEG as an epitaxy precursor, which delivers GaN layers with high intensity photoluminescence and higher electron mobility than those grown with TMG.[17] Some pathways for TEG were investigated previously but no barriers were reported.[13,15] Low-barrier β-hydride elimination seems to play a major role in successful growth procedures and precursors with larger ligands were addressed by experimental and theoretical studies.[15,16,18]

As a common source for group 15 elements *tert*-butylarsine ($AsH_2(t\text{-}C_4H_9)$ TBA) and *tert*-butylphosphine ($PH_2(t\text{-}C_4H_9)$, TBP)[19a] are used as MOVPE precursors. Some decomposition pathways for TBP were computed in an early computational study on the HF level,[19b] supporting the suggestion of breaking of the phosphorous–carbon bond in the initial step.[19c] A concise examination of decomposition pathways of TBP including barriers is not yet available. TEG and TBP fulfill general requirements for MOVPE precursor molecules such as lowered toxicity, suitable lab handling characteristics and, as investigated in this study, well-defined chemical stability.[9]

We want to briefly outline the experimental setup to set the stage for the computational investigations.[20] The original precursors are flushed into the reaction chamber in a hydrogen gas stream at 0.05 atm total pressure. TEG and TBP are kept separated in the gas phase by alternating the precursor flushes with pure hydrogen flushes, which rinse the reaction chamber. This procedure is referred to as flow-rate modulated epitaxy (FME) and was found to produce GaP layers of very high quality.[20] Hence, stable donor–acceptor complexes or oligomers of group 13 and 15 species, which have been extensively revised by Timoshkin and others,[21–25] will presumably not be of major importance for the decomposition. The partial pressures of Ga and P precursors are very low so that the formation of elemental Ga or P clusters[26,27] can be neglected.

The aim of this study is now to investigate a comprehensive reaction catalogue for the important MOVPE precursors TEG and TBP in the hydrogen gas atmosphere[28] *via* accurate computations on the DFT and *ab initio* level providing thermodynamic energies and barriers. To this end, 61 elementary reactions and reaction barriers for a rationally chosen subset of those were calculated on the MP2 and PBE-D3 levels of approximation and checked against benchmark calculations on the CCSD(T) level. The presented decomposition catalogue covers four mechanism classes (homolytical bond cleavage, β-hydrogen decomposition, H_2 and alkane elimination reactions) for unimolecular reactions and three classes (radical recombination, H_2 and alkane elimination reactions) for bimolecular reactions with several reactants. Primarily, this study aims at revealing the resulting decomposition products from the gas phase. Secondly, it presents the chemical mechanisms of the most prominent decomposition classes, showing thermodynamic and kinetic trends for those reactions under experimental conditions. Thirdly, the accurate benchmark data allow an error estimation for production type DFT calculations. This will help both experimental and theoretical scientists to understand the specific decomposition behavior and tune reactor conditions towards clean and complete decomposition.

For the presented results some assumptions had to be formulated which include the limitation of reactions with a maximum of two reaction partners (*e.g.* precursors + H_2), no agglomeration of multiple precursors of the same (due to low partial pressures) and of different types (due to separated input of Ga and P sources, respectively). Furthermore, reactor wall effects and the reactor layout are neglected in this study; however, processes related to the substrate surface will be investigated in future studies.

2. Computational details

Geometry optimizations without symmetry constraints were carried out using the Gaussian09 optimizer (standard convergence criteria)[30] combined with Turbomole (version 6.3.1)[31,32] energies and gradients (SCF convergence criterion 10^{-8} a.u., grid m4). Optimizations were carried out within the density functional approximation applying the GGA functional PBE[33] (widely used in materials science studies)[29] and on an *ab initio* level using the MP2 method. For the PBE calculations, dispersion effects were considered for the calculation of electronic reaction energies and molecular structure optimizations by applying the DFT-D3 method with an improved damping function (further called PBE-D3).[34,35]

One aim of this study is to establish a methodological standard for future studies on the gas phase and surface chemistry in these systems. Therefore, the geometries and energies derived at the MP2 level were used as the gas phase benchmark data for the PBE-D3 calculations of these molecular properties. Complementing the MP2 energies, CCSD(T)[36–39] energies of elementary reactions were derived based on MP2 geometries (on PBE-D3 geometries for transition states) to verify the accuracy of MP2 and PBE-D3. Minimum and transition state structures (the latter characterized by one imaginary mode) were confirmed by calculating the Hessian matrices on PBE-D3 (analytically[40]) and MP2 (numerically[41]). The reactants and products connected by a transition state were identified *via* an intrinsic reaction coordinate (IRC) calculation. Thermodynamic corrections were subsequently derived by statistical thermodynamics in the double harmonic approximation under the assumption of no hindered rotations.[12,42] The results regarding atomic species were complemented with entropic corrections applying the Sackur–Tetrode equation assuming an ideal gas and Maxwell–Boltzmann statistics.[43] The RI approximation was used for all PBE, MP2 and CCSD(T) calculations.[44,45] All methods were used together with a triple-ζ set of Gaussian basis functions (def2-TZVPP).[46] The levels of approximation are denoted PBE-D3/TZ, MP2/TZ and CCSD(T)/TZ in the following. Radical species are denoted by the symbol "•" and found to exhibit doublet spin states with the exception of P• (quartet ground state). All other species involved in this study exhibit a singlet ground state with the exception of $P(t\text{-}C_4H_9)$ and PH (triplet ground state). Maximum deviation of the ideal values

for the $\langle S^2 \rangle$ operator is <0.03 for the radical species, indicating a single-reference character suitable for the unrestricted Kohn–Sham/Hartree–Fock methods applied. The electronic states have been consistently confirmed by the presented PBE-D3, MP2 and CCSD(T) calculations in line with previous results on $GaCH_3$, PH and PH_3.[47,48] The accuracy of the methods applied was measured by comparing the energies to high level CCSD(T)/TZ data and will be presented in the Results section. To our knowledge, experimental thermodynamic data are unfortunately not available for the reactions investigated here. In the ESI,† the structures derived are compared to the available experimental data.[49–52]

3. Results

A catalogue of 61 elementary decomposition reactions was assembled and electronic reaction energies of these reactions were calculated using PBE-D3/TZ, MP2/TZ and CCSD(T)/TZ. Thermodynamic corrections were added for low pressure atmospheres (0.05 atm) and temperatures of 400 °C, 500 °C and 675 °C according to the experimental growth conditions. In the following sections, we present the data for the reaction energies of (i) decomposition of TEG, (ii) decomposition of TBP and (iii) selected transition state energies for TEG and TBP. In the first two sections, uni- and bimolecular reactions are considered separately. Higher order reactions were not considered here due to the low pressure environment. Furthermore, four different possible classes of decomposition reactions were considered for unimolecular reactions: (a) homolytical bond cleavage, (b) β-hydrogen elimination, (c) alkane elimination and (d) H_2 elimination. Three classes were considered for bimolecular decomposition reactions: alkane elimination with (a) a hydrogen radical ($H^\bullet$), (b) alkyl (ethyl, *tert*-butyl) radicals ($C_2H_5^\bullet$, $t\text{-}C_4H_9^\bullet$) or (c) molecular hydrogen (H_2) as reaction partners.

3.1 Thermodynamics of decomposition reactions of TEG

The reaction energies for unimolecular decomposition reactions of TEG are presented in Table 1. Four mechanism classes are listed with elementary reactions of the original precursors and their decomposition products. All reactions shown are endoenergetic ($\Delta E > 0$), while β-hydride and alkane elimination reactions are exergonic ($\Delta G < 0$) for elevated temperatures. This is due to entropic effects resulting in large differences between ΔE and ΔG values. Higher temperatures therefore favor these decomposition reactions. The general ordering (from the least to the most favorable reactions considering ΔE) of the investigated decomposition mechanisms is homolytical cleavage reactions ≪ β-hydride elimination reactions < H_2 elimination reactions < alkane elimination reactions.

The reaction energies for bimolecular decomposition reactions of TEG are presented in Table 2. Here, all reactions listed are energetically accessible. Entropy effects are much smaller since the number of reactants does not change from educts to products (except BG2, BG5). For some radical species the MP2/TZ results deviate considerably from the CCSD(T)/TZ benchmark values (*e.g.* BG3, BG4, BG7) – the differences are mostly less on the PBE/TZ level. This is in line with the known difficulty of the MP2 method to describe radical species accurately. The energetic ordering of decomposition reactions with the following partners (from the least to the most favorable) is alkane elimination reactions with H_2 (BG15-19) < alkane elimination reactions with alkyl radicals (BG12, BG14) < H_2 elimination reactions with $H^\bullet$ radicals (BG9, BG11) < alkane elimination reactions with $H^\bullet$

Table 1 Unimolecular decomposition reactions of TEG and related products. Changes in electronic (ΔE) and Gibbs energy (ΔG) for temperatures of 400 °C (a), 500 °C (b) and 675 °C (c) are given in kJ mol^{-1}. Mechanisms are grouped as homolytical bond cleavage reactions (AG1–AG10), β-hydrogen elimination reactions (AG11–AG14), alkane elimination reactions (AG15–AG17) and H_2 elimination reactions (AG18–AG20)

		PBE-D3/TZ				MP2/TZ				CCSD(T)/TZ
Reaction index	Reaction scheme	ΔE	ΔG (a)	ΔG (b)	ΔG (c)	ΔE	ΔG (a)	ΔG (b)	ΔG (c)	ΔE
AG1	$Ga(C_2H_5)_3 \rightarrow (C_2H_5)_2Ga^\bullet + C_2H_5^\bullet$	292.3	144.3	124.6	90.4	329.4	192.8	174.6	143.2	313.1
AG2	$Ga(C_2H_5)_3 \rightarrow (C_2H_5)_2GaC_2H_4^\bullet + H^\bullet$	404.6	270.8	253.9	224.2	417.4	303.6	289.8	265.4	415.4
AG3	$Ga(C_2H_5)_3 \rightarrow (C_2H_5)_2GaCH_2^\bullet + CH_3^\bullet$	376.2	218.6	198.2	162.6	386.2	246.0	228.2	197.2	365.7
AG4	$(C_2H_5)_2GaC_2H_4^\bullet \rightarrow (C_2H_5)GaC_2H_4 + C_2H_5^\bullet$	201.4	99.4	82.5	53.2	243.9	108.7	89.7	58.2	245.6
AG5	$(C_2H_5)_2Ga^\bullet \rightarrow Ga(C_2H_5) + C_2H_5^\bullet$	144.8	15.3	−1.8	−31.1	167.5	44.5	28.4	0.6	145.1
AG6	$(C_2H_5)_2Ga^\bullet \rightarrow (C_2H_5)GaC_2H_4 + H^\bullet$	313.6	225.9	211.8	187.0	331.8	218.8	204.9	180.4	347.9
AG7	$(C_2H_5)GaC_2H_4 \rightarrow GaC_2H_4^\bullet + C_2H_5^\bullet$	231.2	62.5	43.8	11.4	250.6	118.5	101.1	70.9	210.0
AG8	$Ga(C_2H_5) \rightarrow GaC_2H_4^\bullet + H^\bullet$	400.1	273.1	257.3	229.5	414.9	292.8	277.6	250.7	412.8
AG9	$GaH_3 \rightarrow GaH_2^\bullet + H^\bullet$	337.8	226.9	212.3	186.6	346.8	235.0	220.3	194.5	356.7
AG10	$GaH \rightarrow Ga^\bullet + H^\bullet$	280.4	192.0	179.0	156.0	273.3	183.6	170.6	147.4	288.0
AG11	$Ga(C_2H_5)_3 \rightarrow Ga(C_2H_5)_2H + C_2H_4$	132.9	−13.8	−32.8	−65.6	141.7	13.8	−2.3	−30.2	127.8
AG12	$Ga(C_2H_5)_2H \rightarrow Ga(C_2H_5)H_2 + C_2H_4$	133.7	12.3	−2.9	−29.1	140.4	11.9	−4.3	−32.3	126.8
AG13	$Ga(C_2H_5)H_2 \rightarrow GaH_3 + C_2H_4$	134.8	4.9	−11.6	−40.1	139.3	8.1	−8.5	−37.2	125.9
AG14	$Ga(C_2H_5) \rightarrow GaH + C_2H_4$	140.6	20.6	5.4	−21.1	146.6	24.2	8.7	−18.2	130.4
AG15	$Ga(C_2H_5)_3 \rightarrow Ga(C_2H_5) + n\text{-}C_4H_{10}$	54.5	−47.1	−61.0	−84.8	86.3	−0.6	−12.4	−32.4	68.5
AG16	$(C_2H_5)_2Ga^\bullet \rightarrow GaC_2H_4^\bullet + C_2H_6$	104.4	−12.6	−28.1	−54.8	132.9	26.8	12.6	−11.8	106.7
AG17	$Ga(C_2H_5)H_2 \rightarrow HGa + C_2H_6$	41.5	−51.3	−65.0	−88.5	67.7	−25.8	−39.6	−63.4	55.3
AG18	$Ga(C_2H_5)_2H \rightarrow (C_2H_5)GaC_2H_4 + H_2$	205.1	125.6	111.8	87.9	242.1	127.3	112.1	85.7	247.4
AG19	$Ga(C_2H_5)H_2 \rightarrow Ga(C_2H_5) + H_2$	73.4	−29.4	−44.0	−69.4	93.2	−10.1	−24.7	−50.1	85.4
AG20	$GaH_3 \rightarrow HGa + H_2$	79.3	−13.7	−27.1	−50.4	100.6	6.0	−7.5	−31.2	94.8

Table 2 Bimolecular decomposition reactions of TEG and related products. Changes in electronic (ΔE) and Gibbs energy (ΔG) for temperatures of 400 °C (a), 500 °C (b) and 675 °C (c) are given in kJ mol^{-1}. Mechanisms are grouped as alkane or H_2 elimination reactions with H$^\bullet$ (BG1–BG11), $C_2H_5^\bullet$ (BG12–BG14) or H_2 (BG15–BG19) as a reaction partner

		PBE-D3/TZ				MP2/TZ				CCSD(T)/TZ
Reaction index	Reaction scheme	ΔE	ΔG (a)	ΔG (b)	ΔG (c)	ΔE	ΔG (a)	ΔG (b)	ΔG (c)	ΔE
BG1	$Ga(C_2H_5)_3 + H^\bullet \rightarrow (C_2H_5)_2Ga^\bullet + C_2H_6$	−148.2	−156.6	−159.1	−162.7	−120.2	−117.7	−118.8	−120.0	−138.1
BG2	$(C_2H_5)_2Ga^\bullet + H^\bullet \rightarrow Ga(C_2H_5)_2H$	−330.2	−226.0	−212.1	−187.8	−343.6	−227.9	−212.3	−185.1	−352.9
BG3	$(C_2H_5)_2Ga^\bullet + H^\bullet \rightarrow Ga(C_2H_5) + C_2H_6$	−295.6	−285.6	−285.4	−284.3	−282.0	−266.0	−265.0	−262.5	−306.1
BG4	$Ga(C_2H_5)_2H + H^\bullet \rightarrow Ga(C_2H_5)H^\bullet + C_2H_6$	−144.2	−132.2	−131.5	−129.5	−120.0	−111.5	−111.6	−111.0	−137.6
BG5	$Ga(C_2H_5)H^\bullet + H^\bullet \rightarrow Ga(C_2H_5)H_2$	−333.4	−224.4	−209.9	−184.5	−345.0	−235.9	−221.5	−196.2	−354.4
BG6	$Ga(C_2H_5)H^\bullet + H^\bullet \rightarrow GaH + C_2H_6$	−291.9	−275.7	−274.9	−273.0	−277.2	−261.7	−261.1	−259.5	−299.1
BG7	$Ga(C_2H_5)H_2 + H^\bullet \rightarrow GaH_2^\bullet + C_2H_6$	−138.7	−137.0	−137.7	−138.3	−119.4	−116.2	−116.9	−117.6	−136.3
BG8	$Ga(C_2H_5) + H^\bullet \rightarrow Ga^\bullet + C_2H_6$	−190.3	−156.3	−154.1	−149.9	−185.5	−151.4	−149.5	−145.6	−200.4
BG9	$GaH_3 + H^\bullet \rightarrow GaH_2^\bullet + H_2$	−101.0	−99.4	−99.8	−100.2	−86.5	−84.4	−84.8	−85.3	−96.8
BG10	$GaH_2^\bullet + H^\bullet \rightarrow GaH + H_2$	−258.5	−240.6	−239.4	−237.1	−246.2	−229.0	−227.8	−225.6	−261.8
BG11	$GaH + H^\bullet \rightarrow Ga^\bullet + H_2$	−158.4	−134.4	−133.1	−130.8	−159.9	−135.8	-134.6	−132.4	−165.4
BG12	$Ga(C_2H_5)_3 + C_2H_5^\bullet \rightarrow Ga(C_2H_5)_2^\bullet + n\text{-}C_4H_{10}$	−90.3	−62.4	−59.3	−53.7	−81.3	−45.1	−40.8	−33.1	−76.5
BG13	$(C_2H_5)_2Ga^\bullet + C_2H_5^\bullet \rightarrow (C_2H_5)GaC_2H_4 + C_2H_6$	−126.8	−75.0	−71.9	−66.2	−117.7	−91.6	−88.5	−82.7	−103.3
BG14	$Ga(C_2H_5) + C_2H_5^\bullet \rightarrow GaC_2H_4^\bullet + C_2H_6$	−40.4	−27.8	−26.3	−23.7	−34.6	−17.7	−15.8	−12.4	−38.4
BG15	$Ga(C_2H_5)_3 + H_2 \rightarrow Ga(C_2H_5)_2H + C_2H_6$	−39.6	−56.3	−59.1	−63.6	−30.5	−26.2	−26.0	−25.2	−37.6
BG16	$Ga(C_2H_5)_2H + H_2 \rightarrow Ga(C_2H_5)H_2 + C_2H_6$	−38.8	−30.2	−29.2	−27.1	−31.7	−28.0	−27.9	−27.3	−38.6
BG17	$Ga(C_2H_5)H_2 + H_2 \rightarrow GaH_3 + C_2H_6$	−37.7	−37.6	−37.9	−38.0	−32.9	−31.8	−32.1	−32.2	−39.5
BG18	$Ga(C_2H_5) + H_2 \rightarrow GaH + C_2H_6$	−31.9	−21.9	−21.0	−19.1	−25.5	−15.7	−14.9	−13.3	−30.1
BG19	$Ga(C_2H_5)_2^\bullet + H_2 \rightarrow Ga(C_2H_5)H^\bullet + C_2H_6$	−35.7	−31.9	−31.5	−30.4	−30.3	−20.0	−18.8	−16.3	−37.1

radicals (BG1, BG4, BG7, BG8) ≪ radical recombinations (with or without elimination products; BG2, BG3, BG5, BG6, BG10, BG13). Reactions AG11–AG14 (β-hydride elimination reactions), AG19 and AG20 (H_2 elimination reactions), AG15 and AG17 (alkane elimination reactions) and BG15–BG18 (alkane elimination reactions with H_2) were chosen for subsequent investigation of reaction barriers under the condition of low H$^\bullet$ concentration.

3.2 Thermodynamics of decomposition reactions of TBP

The reaction energies for unimolecular decomposition reactions of TBP are presented in Table 3. Most of the reactions are energetically and thermodynamically unfavorable. Only β-hydrogen elimination reactions (AP6 and AP7) are exothermic, although the entropy effects are very large for all unimolecular reactions. For the P-containing species a good agreement was found between the computational methods applied except for AP9 and AP12 which can be attributed to the difficulty of DFT dealing with atomic species. The reaction energies for bimolecular decomposition reactions of TBP are presented in Table 4. All elimination reactions are energetically (except BP8) and thermodynamically accessible. As for the bimolecular reactions with Ga species, entropic effects are small (except BP8, which results in three species). Reactions AP6 (β-hydrogen elimination) and BP8 (alkene + H_2 elimination with H_2) were chosen for the subsequent transition state analysis. No transition state could be found for reaction BP7.

Table 3 Unimolecular decomposition reactions of TBP and related products. Changes in electronic (ΔE) and Gibbs energy (ΔG) for temperatures of 400 °C (a), 500 °C (b) and 675 °C (c) are given in kJ mol^{-1}. Mechanisms are grouped as homolytical bond cleavage reactions (AP1–AP5), β-hydrogen elimination reactions (AP6 and AP7), alkane elimination reactions (AP8 and AP9) and H_2 elimination reactions (AP10–AP12)

		PBE-D3/TZ				MP2/TZ				CCSD(T)/TZ
Reaction index	Reaction scheme	ΔE	ΔG (a)	ΔG (b)	ΔG (c)	ΔE	ΔG (a)	ΔG (b)	ΔG (c)	ΔE
AP1	$P(t\text{-}C_4H_9)H_2 \rightarrow P(t\text{-}C_4H_9)H^\bullet + H^\bullet$	349.7	230.9	215.5	188.3	352.2	231.6	216.0	188.6	357.4
AP2	$P(t\text{-}C_4H_9)H_2 \rightarrow PH_2^\bullet + t\text{-}C_4H_9^\bullet$	279.3	119.9	99.1	62.9	314.4	156.6	135.8	99.8	289.2
AP3	$P(t\text{-}C_4H_9)H^\bullet \rightarrow PH + t\text{-}C_4H_9^\bullet$	266.1	126.6	108.0	75.8	281.4	143.7	125.3	93.2	260.7
AP4	$PH_3 \rightarrow H_2P^\bullet + H^\bullet$	356.9	239.9	224.8	198.2	353.3	234.6	219.4	192.7	360.1
AP5	$PH \rightarrow P^\bullet + H^\bullet$	313.8	218.9	205.6	181.9	277.6	181.6	168.2	144.4	295.8
AP6	$P(t\text{-}C_4H_9)H_2 \rightarrow PH_3 + i\text{-}C_4H_8$	96.9	−48.7	−67.6	−100.5	111.7	−36.3	−55.7	−89.3	96.3
AP7	$P(t\text{-}C_4H_9) \rightarrow PH + i\text{-}C_4H_8$	111.4	−20.8	−38.0	−67.9	114.1	−21.4	−39.1	−69.9	100.9
AP8	$P(t\text{-}C_4H_9)H_2 \rightarrow PH + i\text{-}C_4H_{10}$	205.9	90.6	73.3	46.2	199.0	81.6	65.0	36.3	184.4
AP9	$P(t\text{-}C_4H_9)H^\bullet \rightarrow P^\bullet + i\text{-}C_4H_{10}$	170.0	78.7	64.5	39.8	124.5	31.7	17.2	−7.8	122.8
AP10	$P(t\text{-}C_4H_9)H_2 \rightarrow P(t\text{-}C_4H_9) + H_2$	239.9	123.2	107.4	79.9	236.8	119.0	103.1	75.5	231.0
AP11	$PH_3 \rightarrow PH + H_2$	254.5	151.1	137.1	112.5	239.2	133.9	119.7	94.9	235.7
AP12	$PH_2^\bullet \rightarrow P^\bullet + H_2$	211.5	130.2	117.9	96.1	163.5	80.9	68.5	46.7	171.4

Table 4 Bimolecular decomposition reactions of TBP and related products. Changes in electronic (ΔE) and Gibbs energy (ΔG) for temperatures of 400 °C (a), 500 °C (b) and 675 °C (c) are given in kJ mol^{-1}. Mechanisms are grouped as alkane/alkene and/or H_2 elimination reactions with H$^\bullet$ (BP1–BP5), t-$C_4H_9^\bullet$ (BP6) or H_2 (BP7–BP10) as a reaction partner

		PBE-D3/TZ				MP2/TZ				CCSD(T)/TZ
Reaction index	Reaction scheme	ΔE	ΔG (a)	ΔG (b)	ΔG (c)	ΔE	ΔG (a)	ΔG (b)	ΔG (c)	ΔE
BP1	$P(t\text{-}C_4H_9)H_2 + H^\bullet \rightarrow P(t\text{-}C_4H_9)H^\bullet + H_2$	−89.1	−95.5	−96.7	−98.6	−81.1	−87.8	−89.2	−91.2	−96.0
BP2	$P(t\text{-}C_4H_9)H_2 + H^\bullet \rightarrow PH_2^\bullet + i\text{-}C_4H_{10}$	−130.6	−147.0	−150.1	−154.9	−120.1	−137.1	−140.5	−145.8	−144.6
BP3	$P(t\text{-}C_4H_9) + H^\bullet \rightarrow P^\bullet + i\text{-}C_4H_{10}$	−159.0	−140.0	−139.6	−138.7	−193.4	−175.2	−175.1	−174.6	−204.2
BP4	$PH_3 + H^\bullet \rightarrow PH_2^\bullet + H_2$	−81.9	−86.5	−87.3	−88.6	−80.0	−84.8	−85.7	−87.1	−93.4
BP5	$PH + H^\bullet \rightarrow P^\bullet + H_2$	−125.0	−107.4	−106.6	−105.0	−155.7	−137.8	−136.9	−135.4	−157.7
BP6	$P(t\text{-}C_4H_9)H_2 + t\text{-}C_4H_9^\bullet \rightarrow P(t\text{-}C_4H_9)H^\bullet + i\text{-}C_4H_{10}$	−60.2	−36.0	−33.7	−29.6	−82.4	−62.1	−60.3	−57.0	−76.3
BP7	$P(t\text{-}C_4H_9)H_2 + H_2 \rightarrow PH_3 + i\text{-}C_4H_{10}$	−48.6	−60.5	−62.8	−66.3	−40.2	−52.3	−54.8	−58.7	−51.2
BP8	$P(t\text{-}C_4H_9)H_2 + H_2 \rightarrow PH_3 + i\text{-}C_4H_8 + H_2$	96.9	−48.7	−67.6	−100.5	111.7	−36.3	−55.7	−89.3	96.7
BP9	$P(t\text{-}C_4H_9)H^\bullet + H_2 \rightarrow PH_2^\bullet + i\text{-}C_4H_{10}$	−41.5	−51.5	−53.4	−56.3	−39.0	−49.2	−51.3	−54.5	−48.6
BP10	$P(t\text{-}C_4H_9) + H_2 \rightarrow PH + i\text{-}C_4H_{10}$	−34.1	−32.6	−33.1	−33.7	−37.8	−37.4	−38.2	−39.3	−46.5

To summarize the part of the study focusing on the reaction energies: unimolecular decomposition reactions exhibit much larger changes in ΔG upon considering increasing temperatures compared to bimolecular reactions. As expected, all reactions leading from radical species to saturated products are exergonic (see also ref. 10) while larger radical species tend to be more stabilized than small ones. All β-hydrogen elimination reactions (alkene elimination reactions) are exergonic (Ga and P species) and so are many uni- and bimolecular alkane and H_2 elimination reactions from Ga species. All unimolecular H_2 and alkane eliminations from P species are endergonic. This catalogue's bimolecular decomposition reactions are, generally, exergonic. Gas phase reactivity cannot be understood from the thermodynamic data alone. However, they give a strong hint on which reaction classes are relevant for the investigation of reaction kinetics in terms of transition state theory. This will be described for the reactions indicated in the previous paragraphs in the next section.

3.3 Transition states of TEG and TBP decomposition reactions

Several elementary decomposition reactions were identified from the catalogue presented in Tables 1–4, where the thermodynamic data indicate their importance for the gas phase decomposition chemistry of the MOVPE growth of GaP. For those reactions, transition states linking reactants and products of the reactions in Tables 1–4 were investigated. Subsequently, the possible decomposition pathways were formulated which determine the possible decomposition products. Furthermore, those pathways contain the structural data which provide rationalization of the underlying reaction mechanisms.

The selection criteria for the reactions considered in this section are the following: (i) elementary steps are exergonic, (ii) they do not depend on any other species than the carrier gas H_2 (which is present in sufficient concentration), and (iii) the reactant species will realistically be available either as original precursors or *via* exclusively exergonic preceding reactions. The transition states (TS) were optimized with PBE-D3/TZ.

Table 5 Transition state data for selected decomposition reactions of TEG, TBP and related products at PBE-D3/TZ. Electronic energies of activation ($\Delta E^\#$) and Gibbs energy of activation ($\Delta G^\#$) for temperatures of 400 °C (a), 500 °C (b) and 675 °C (c) are given in kJ mol^{-1}. The transition states' imaginary vibrational mode (ν_{imag}) is given in cm^{-1}. Reactions AG11–AG14 and AP6 represent unimolecular β-hydrogen, AG15–AG17 and AG19–AG20 represent unimolecular alkane and H_2 elimination reactions, respectively. BG15–BG18 and BP8 represent bimolecular alkane and H_2 elimination reactions, respectively

Reaction index	Reaction scheme	$\Delta E^\#$	$\Delta G^\#$ (a)	$\Delta G^\#$ (b)	$\Delta G^\#$ (c)	ν_{imag}	$\Delta E^\#$ MP2/TZ//PBE-D3/TZ[a]	$\Delta E^\#$ CCSD(T)/TZ//PBE-D3/TZ[a]
AG11	$Ga(C_2H_5)_3 \rightarrow Ga(C_2H_5)_2H + C_2H_4$	131.6	141.0	144.3	150.2	i648	152.6	147.5
AG12	$Ga(C_2H_5)_2H \rightarrow Ga(C_2H_5)H_2 + C_2H_4$	128.1	149.9	155.1	164.2	i686	150.7	145.3
AG13	$Ga(C_2H_5)H_2 \rightarrow GaH_3 + C_2H_4$	123.8	129.2	131.9	136.7	i717	149.6	143.3
AG14	$Ga(C_2H_5) \rightarrow GaH + C_2H_4$	87.2	82.6	84.1	86.8	i430	111.5	109.7
AG15	$Ga(C_2H_5)_3 \rightarrow Ga(C_2H_5) + n\text{-}C_4H_{10}$	312.3	326.2	329.4	335.1	i377	375.3	360.1
AG17	$Ga(C_2H_5)H_2 \rightarrow HGa + C_2H_6$	194.7	199.8	202.2	206.7	i713	234.2	236.9
AG19	$Ga(C_2H_5)H_2 \rightarrow Ga(C_2H_5) + H_2$	217.0	215.6	216.8	219.1	i1140	271.2	255.7
AG20	$GaH_3 \rightarrow HGa + H_2$	211.5	200.5	200.5	200.4	i1025	269.0	251.4
BG15	$Ga(C_2H_5)_3 + H_2 \rightarrow Ga(C_2H_5)_2H + C_2H_6$	96.7	208.5	225.2	254.5	i1233	126.2	124.7
BG16	$Ga(C_2H_5)_2H + H_2 \rightarrow Ga(C_2H_5)H_2 + C_2H_6$	93.7	217.0	235.4	267.6	i1258	124.3	122.8
BG17	$Ga(C_2H_5)H_2 + H_2 \rightarrow GaH_3 + C_2H_6$	92.1	204.7	221.5	251.0	i1283	124.3	122.6
BG18	$Ga(C_2H_5) + H_2 \rightarrow GaH + C_2H_6$	67.3	169.2	184.8	212.0	i1156	105.4	107.3
AP6	$P(t\text{-}C_4H_9)H_2 \rightarrow PH_3 + i\text{-}C_4H_8$	242.6	217.4	216.2	214.1	i648	310.5	293.1
BP8	$P(t\text{-}C_4H_9)H_2 + H_2 \rightarrow PH_3 + i\text{-}C_4H_8 + H_2$	264.6	337.3	350.1	372.4	i1120	365.8	354.0

[a] Energy calculations based on PBE-D3/TZ structures.

The electronic activation energies of the selected reactions and the frequencies of the transition state modes are given in Table 5. The energies vary from 67.3 (BG18) to 312.3 kJ mol^{-1} (AG15), exemplifying the strong differences between barriers for different mechanisms. It becomes clear that the barriers for TEG and derived species are much lower compared to the two barriers investigated for decomposition reactions of TBP (except AG15). It is also striking that entropy has a much smaller influence on the barrier height compared to the reaction energies (Tables 1–4), except for the bimolecular reactions involving H_2 (BG15–BG18, BP8), where the barriers are drastically increased by the inclusion of entropic effects. This can be understood in terms of the entropy-lowering association of two species to one transition structure in the bimolecular case. The vibrational modes of the TS structures connecting educts and products can also be taken to distinguish the different mechanism classes: transition states containing H_2 exhibit much higher mode energies (>1100 cm^{-1}) compared to alkane elimination reactions (377–717 cm^{-1}). Before discussing the implications of the reaction catalogue introduced, an evaluation of the accuracy for the methods chosen will be presented.

3.4 Accuracy of PBE-D3/TZ and MP2/TZ *vs.* CCSD(T)/TZ

In order to validate the accuracy of the broadly applicable PBE-D3/TZ and MP2/TZ methods, statistical data regarding the deviations from the highly accurate CCSD(T)/TZ computations are given in Table 6. All presented deviation criteria of PBE-D3/TZ energies are of the same order as the respective deviations of MP2/TZ energies with respect to CCSD(T)/TZ//MP2/TZ. This validation of PBE-D3 is important as for calculations of larger systems the application of DFT-based methods will be preferred over the costly post-HF methods, especially for investigation of surface-assisted reactions where the MP2 method is currently only feasible for small systems. Energies of reactions where radical species are involved have a larger deviation and represent the respective maximum absolute deviations of this catalogue's reactions. This is known for species with an unpaired electron and mainly due to the inaccurate exchange contribution to the energy in GGA exchange–correlation functionals.[54] However, focusing on decomposition reaction energies, the description of even large radicals by PBE-D3/TZ seems to be of sufficient accuracy relative to CCSD(T)/TZ.

The relative and absolute deviations of the examined energy barriers are larger, as it is known for GGA functionals to underestimate reaction barriers.[55] Remarkably, RMS, RAD and MAE of PBE-D3/TZ are smaller compared to MP2/TZ with respect to CCSD(T)/TZ. This overestimation of activation energies is a known shortcoming of MP2. Similar trends of reaction energy deviations for DFT relative to CCSD(T)/TZ were also found in other studies on Ga precursor decomposition.[12] In conclusion, the accuracy of the methods is sufficient for the purpose of identifying relevant decomposition products and analyzing the respective mechanisms.

In the following, uni- and bimolecular decomposition schemes including mainly exergonic reactions are presented for TEG and TBP. From those schemes several pathways were assembled involving the reaction energies together with the reaction barriers presented above.

3.5 Decomposition scheme for TEG

In the light of the results given in Tables 1 and 2, the plethora of possible reactions is reduced to the following set: unimolecular β-hydride elimination reactions or homolytical bond cleavage reactions of Ga–C, C–C or C–H can be formulated for TEG. Furthermore, recombinative elimination reactions of alkanes or hydrogen are energetically accessible for some decomposition products. In the bimolecular case, alkane and H_2 elimination reactions are possible with reactants like H_2 or radicals ($H^\bullet$, $C_2H_5^\bullet$). This leads to the decomposition pathways of first (Fig. 1, top) and second (Fig. 1, bottom) order reactions. However, all homolytical cleavage reactions of saturated species are endoenergetic and endergonic and are not considered further in this study. Specifically, the bond energies for TEG were calculated to be 404.6 kJ mol^{-1} for the terminal C_β–H bond, 376.2 kJ mol^{-1} for the C_α–C_β bond and 292.3 kJ mol^{-1} for the Ga–C bond (AG2, AG3, AG1 for PBE-D3/TZ in Table 1). As a consequence, the remaining pathways build a decomposition scheme for TEG. The major pathways are discussed in the following subsections in detail.

Pathway 1, "β-hydride eliminations". The possibility of reaction *via* β-hydride elimination is a significant advantage to TEG compared to, for instance, TMG which has been studied extensively for CVD applications.[12] Since a carbon atom in the β-position to gallium is absent in TMG, only endergonic homolytical cleavage reaction can occur, hence a decomposition reaction is less likely.[15] The suggested decomposition pathway 1 for TEG has four elementary steps and leads to

Table 6 Statistical deviation of PBE-D3/TZ and MP2/TZ reaction energies (ΔE) w.r.t. CCSD(T)/TZ energies and barriers ($\Delta E^{\#}$) w.r.t. CCSD(T)/TZ and MP2/TZ energies. *Method1//method2* indicates an energy calculation by *method1* on the structure optimized with *method2*

	Reaction energies						Reaction barriers	
	PBE-D3 w.r.t. CCSD(T)//MP2			MP2 w.r.t. CCSD(T)//MP2			PBE-D3 w.r.t. CCSD(T)//PBE-D3	PBE-D3 w.r.t. MP2//PBE-D3
	All	Radicals	Non-rad.	All	Radicals	Non-rad.	All	All
RMS[a]	17.7	19.5	13.6	14.4	15.8	11.0	40.8	48.7
MAE[b]	−47.2	−47.2	42.4	−40.6	−40.6	−17.7	89.5	101.2
RAD[c]	12.0	12.0	11.9	12.0	10.3	14.4	20.4	22.3
RMD[d]	−38.5	−38.5	24.9	−25.9	−19.3	−25.9	37.3	36.2

[a] Root mean square error in kJ mol^{-1}. [b] Maximum absolute error in kJ mol^{-1}. [c] Relative average deviation in %. [d] Relative maximum deviation in %.

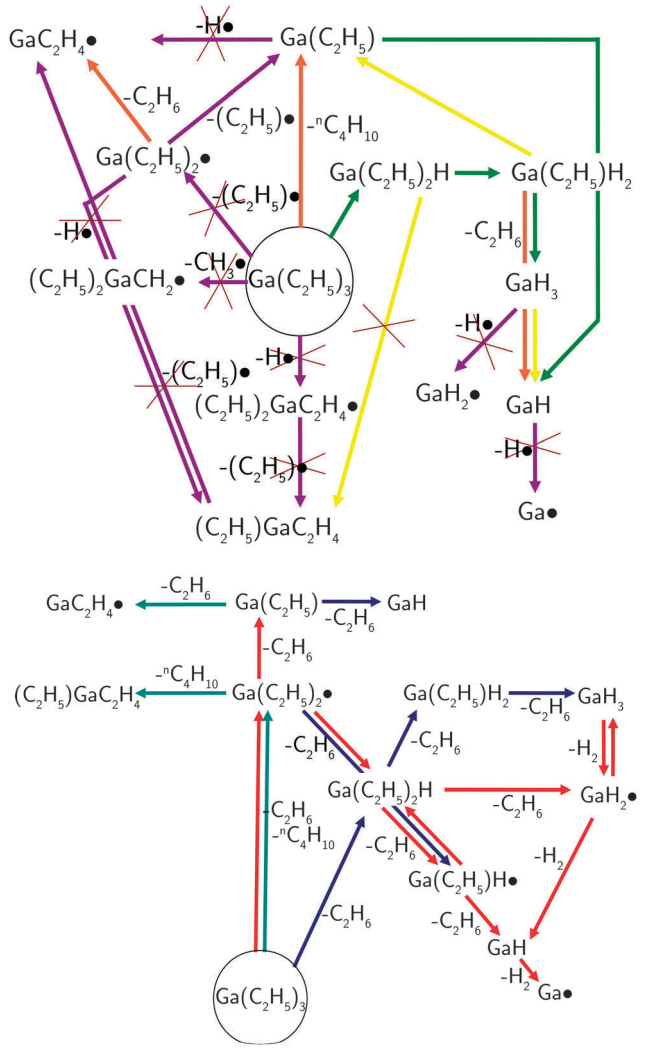

Fig. 1 Unimolecular (top) and bimolecular (bottom) decomposition reaction schemes for TEG considering information from Tables 1 and 2. Endergonic steps (at 400 °C) are crossed out or do not appear at all. Decomposition mechanisms are classified as radical cleavage reactions (magenta), alkane (orange), H_2 (yellow) and β-hydride (green) elimination reactions. Bimolecular elimination of alkanes or H_2 is considered with the $H^\bullet$ (red) or $C_2H_5^\bullet$ (turquoise) radicals or H_2 (blue) as reaction partners.

GaH as the smallest thermodynamically accessible Ga species (see Fig. 2). Firstly, ethylene is eliminated from TEG in a β-hydride elimination step with a Gibbs energy barrier of $\Delta G^{\#}_{400}$ = 141.0 kJ mol^{-1}. The transition state is rather symmetric with d(Ga–H) = 1.697 Å and d(C–H) = 1.718 Å. The same is true for the following further β-hydride elimination steps with barriers of $\Delta G^{\#}_{400}$ = 149.9 and $\Delta G^{\#}_{400}$ = 129.2 kJ mol^{-1}, respectively, leading to GaH_3. A reduction in the Ga–C, Ga–H and H–C bond lengths thereby points to slightly earlier transition states for the less substituted Ga species. And indeed, the trend in electronic barriers ($\Delta E^{\#}$ = 131.6, 128.1 and 123.8 kJ mol^{-1}, Table 1) confirms this assumption. Entropy covers this effect and leads to the observed different trend in $\Delta G^{\#}$. The fourth step within this pathway exhibits the highest barrier. The H_2 elimination from GaH_3 is slightly exergonic and has a barrier of $\Delta G^{\#}_{400}$ = 200.5 kJ mol^{-1}. The subsequent homolytical cleavage to $Ga^\bullet$ and $H^\bullet$ is highly endergonic in the gas phase (ΔG_{400} = 192.0 kJ mol^{-1}, see Table 1). Hence, *via* this pathway GaH_3 will likely be the main product with the possibility of GaH at elevated temperatures. From the graphical representation, it appears that the differences in the reaction profile with an increase in temperature might be due to entropy effects on the transition states. But a closer analysis of the numbers in Tables 1 and 5 reveals that the temperature effects of the intermediates are much stronger compared to the transition states.

Pathway 2, "*n*-butane elimination". A recombinative elimination of *n*-butane from TEG leads to monoethylgallium ($Ga(C_2H_5)$) in a single step (Fig. 3), but the barrier for this reaction is very large ($\Delta G^{\#}_{400}$ = 326.2 kJ mol^{-1}) and unlikely to be surmounted even at elevated temperatures. If monoethylgallium can be formed by any (*e.g.* surface-assisted) process, a β-hydride elimination reaction may result in gallium monohydride (GaH) in a low barrier step ($\Delta G^{\#}_{400}$ = 82.6 kJ mol^{-1}). GaH is an interesting intermediate as it can be formed from many different sources (see Fig. 1).

Pathway 3, "monoethylgallane decomposition processes". Next to the low-barrier β-hydride elimination described in pathway 1, monoethylgallane can directly decompose to GaH (Fig. 4, reaction to the right) by the elimination of ethane ($\Delta G^{\#}_{400}$ = 199.8 kJ mol^{-1}). Furthermore, H_2 elimination to $Ga(C_2H_5)$ (Fig. 4, reaction to the left) can occur with a higher barrier of $\Delta G^{\#}_{400}$ = 215.6 kJ mol^{-1}. Since both processes are thermodynamically and kinetically less favorable than the β-hydride elimination (Fig. 2), they are not highly relevant gas phase reactions.

Pathway 4, "2nd order pathway, ethane elimination". The bimolecular decomposition reactions with a radical reactant or H_2 are exergonic. A highly interlinked decomposition network can be formulated (Fig. 1, bottom) leading to both radical and non-radical products. Formally, atomic Ga can be reached *via* an alkane elimination pathway with hydrogen radicals $H^\bullet$ as reactants (*e.g.* ΔG_{400}(BG1) = −156.6 kJ mol^{-1}, Table 2). Assuming low concentrations of these radicals in the gas phase for thermodynamic reasons (H_2 dissociation: ΔG_{400} = 326.4 kJ mol^{-1}) no barrier was calculated for such elimination steps. Reactions with molecular hydrogen (H_2), which is used as a carrier gas and available in high concentrations, are more likely. The pathway shown in Fig. 5 contains three steps of H_2 addition reactions to saturated Ga species, which decompose under simultaneous ethane elimination in subsequent steps to $Ga(C_2H_5)_2H$, $Ga(C_2H_5)H_2$ and GaH_3, respectively. Note that electronic barriers are lower throughout compared to the corresponding unimolecular β-hydride elimination barriers of these species (Table 5), although an additional H–H bond is broken. However, upon applying thermodynamic corrections to the transition state energies of this bimolecular decomposition class the barriers are drastically increased. The very high initial barrier for the H_2-assisted reaction (BG1, $\Delta G^{\#}_{400}$ = 208.5 kJ mol^{-1}) indicates that the decomposition reactions *via* second-order reactions are less important.

Comparing uni- and bimolecular alkyl elimination from gallane species (Fig. 2 and 5), yet another trend can be

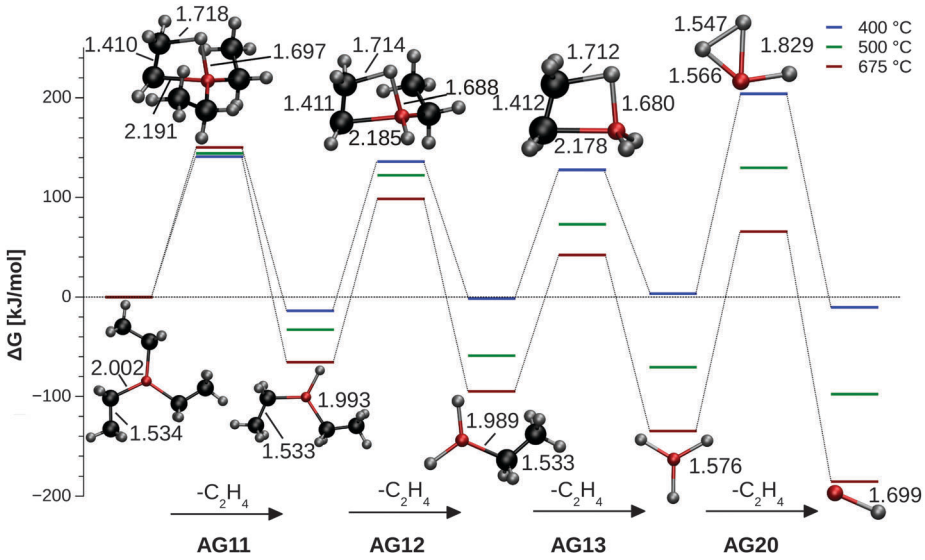

Fig. 2 Three-step β-hydride elimination from TEG to gallane (GaH_3), followed by a H_2 elimination step to GaH. Changes in Gibbs energy (ΔG) and barriers relative to the respective reactants (in kJ mol^{-1}) at experimental temperatures. Distances are given in Å.

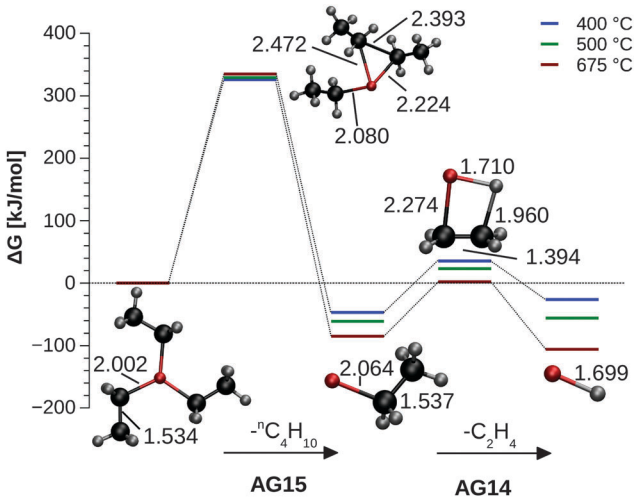

Fig. 3 Two-step decomposition of TEG to GaH *via* $Ga(C_2H_5)$. Changes in Gibbs energy (ΔG) and barriers relative to the respective reactants (in kJ mol^{-1}) at experimental temperatures. Distances are given in Å.

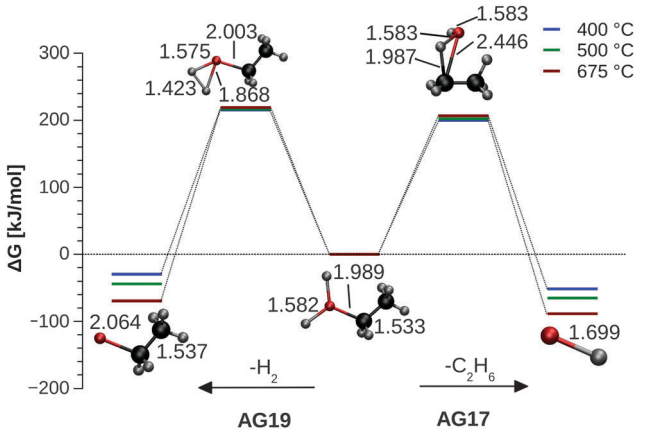

Fig. 4 Monoethylgallane (middle) decomposition to $Ga(C_2H_5)$ (left path) and GaH (right path). Changes in Gibbs energy (ΔG) and barriers (in kJ mol^{-1}) at experimental temperatures. Distances are given in Å.

observed: while the thermodynamics of unimolecular β-hydride elimination reactions strongly depend on temperature (Fig. 2), this is not the case for the bimolecular C_2H_6 elimination of the same species (Fig. 5). On the other hand, the barriers are significantly increasing with an increase in temperature for the bimolecular classes, whereas the unimolecular barriers are not affected by temperature (see also Table 5).

3.6 Decomposition scheme for TBP

Building upon the data presented in Tables 3 and 4, a decomposition scheme for TBP (Fig. 6) can be set up similar to TEG (Fig. 1). The reaction energies lead to the conclusion that TBP can decompose *via* homolytical bond cleavage and the elimination of hydrogen gas, alkane or alkene compounds, respectively. As it turns out, most unimolecular reactions (Fig. 6, left) can be neglected, since they are strongly endergonic (Table 3). Considering reactions with H_2, a hydrogen or an alkyl radical (*e.g.* $H^{\bullet}$, $t\text{-}C_4H_9^{\bullet}$), a bimolecular decomposition scheme of exclusively exergonic reactions can be formulated which involves radical and non-radical intermediate species. Within this scheme (Fig. 6, right), no P species smaller than the radical $PH_2^{\bullet}$ can be reached from TBP. If dehydrogenated $P(t\text{-}C_4H_9)$ is present, PH and atomic P can be reached on exergonic paths. The major pathways are discussed in the following.

Pathway 5 "β-hydrogen elimination". Fan *et al.* propose an "intramolecular β-hydrogen elimination" mechanism for TBP, confirmed by temperature-dependent FT-IR measurements performed during MOVPE in a H_2 atmosphere similar to the conditions in our study.[56] This exergonic alkene elimination (i-C_4H_8, isobutene) is the only unimolecular decomposition mechanism considered here as all other classes are highly

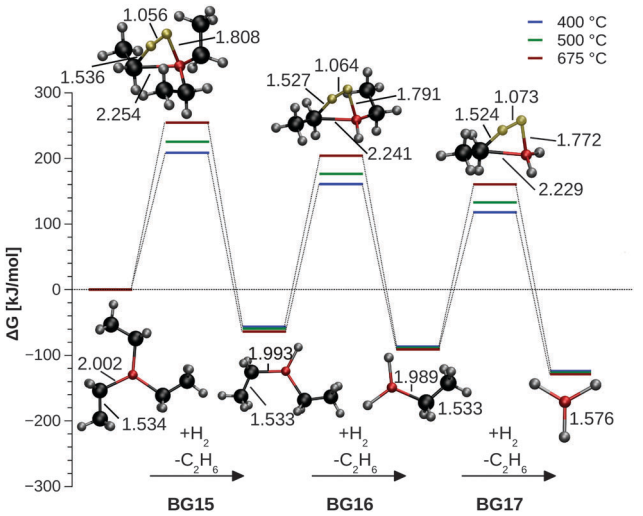

Fig. 5 Bimolecular C_2H_6 elimination reactions of $Ga(C_2H_5)_nH_{(3-n)}$ (n = 3, 2, 1) with a reaction partner H_2. Changes in Gibbs energy (ΔG) and barriers relative to the respective reactants (in kJ mol^{-1}) at experimental temperatures. Distances are given in Å.

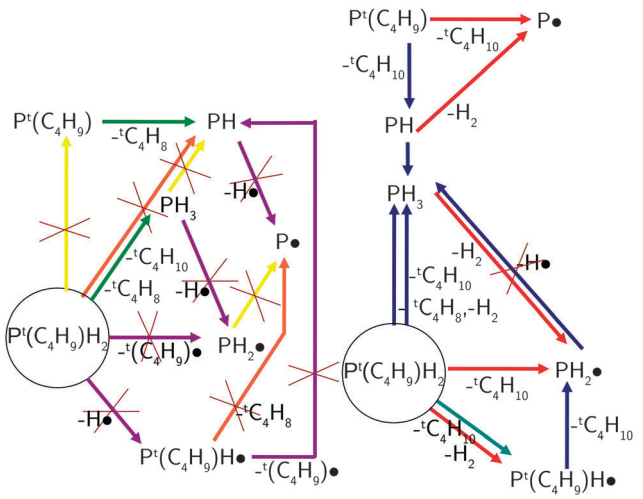

Fig. 6 Unimolecular (left) and bimolecular (right) decomposition reaction schemes for TBP considering information from Tables 3 and 4. Endergonic steps (at 400 °C) are crossed out or do not appear at all. Decomposition mechanisms are classified as radical cleavage reactions (magenta), alkane (orange), H_2 (yellow) and β-hydrogen (green) elimination reactions. Bimolecular elimination of alkanes and/or H_2 is considered with the H• (red) or t-C_4H_9• (turquoise) radicals or H_2 (blue) as reaction partners.

endergonic. It can be formulated for TBP as well as for the triplet species P(t-C_4H_9) (AP6 and AP7). It involves the transfer of a hydrogen atom from a β-carbon atom of the butyl group to the phosphorous center. As the formal acceptor orbital of the P atom is occupied, the reaction cannot directly be compared to the β-hydride mechanism discussed for the Ga species (which exhibits an empty p-orbital).[57] A transition state with a rather large P–C distance was found (left path in Fig. 7). A detailed analysis of this reaction class is beyond the scope of this study and will be presented elsewhere.[58] The barrier for this reaction (AP6, $\Delta G^{\#}_{400}$ = 217.4 kJ mol^{-1}) is significantly higher than typical barriers of the calculated β-hydride elimination of Ga species (AG11–AG14, $\Delta G^{\#}_{400}$ = 82.6–149.9 kJ mol^{-1}). Furthermore, the trend of Gibbs energy barriers for the reaction with an increase in temperature is reversed with respect to the Ga β-hydride eliminations indicating differences in the mechanism. The equivalent decomposition from the triplet P(t-C_4H_9) will not be discussed in detail here since its formation from TBP by eliminating H_2 is endergonic (AP10, ΔG_{400} = 123.2 kJ mol^{-1}).

Pathway 6, "second order pathway, alkane elimination". The bimolecular decomposition network of TBP is less interlinked compared to the bimolecular network of Ga species, since only a small number of decomposition products can be formulated. Reactions of TBP with a radical may lead to P(t-C_4H_9)H• or PH_2•, from which recombination with further radical partners (*e.g.* H•) may lead to the original precursor or phosphine (PH_3). The most important bimolecular decomposition pathway for TBP is the exergonic concerted elimination of isobutene and H_2. A transition state can be found for this single-step reaction and is very high in energy (BP8, $\Delta E^{\#}$ = 264.6 kJ mol^{-1}). As expected for a bimolecular reaction, the unfavorable entropy factor increases this barrier even further to $\Delta G^{\#}_{400}$ = 337.3 kJ mol^{-1} rendering it highly improbable that this barrier could be overcome at the given temperature (see the right path in Fig. 7). Several bimolecular reactions can be formulated for P(t-C_4H_9), but applying the assumption given above (low reactant concentration due to missing decomposition pathways of TBP to this intermediate) no reaction barrier was calculated for these. Considering the thermodynamic schemes of both uni- and bimolecular decomposition pathways from TBP, only phosphine (PH_3) is likely to be formed in significant concentrations aside the original precursor in the gas phase. Notably, it is known from the experiment that the fraction of the original precursor finally arriving on the surface is very large for P species[4,56] in line with the large barriers presented here.

4. Discussion

The results presented in the previous sections will be discussed in the light of the assumptions presented earlier. In the first Results section, thermodynamic data were presented for many elementary reactions starting from the precursors TEG ($Ga(C_2H_5)_3$) and TBP ($PH_2(t$-$C_4H_9)$). Of course, it cannot be excluded that a reaction might be missing in the catalogue but considering the large amount of data and the various mechanism classes we are confident to have included the important reactions. Initially, all fragments were further investigated even when no direct route to this fragment was found. This enables a complete picture of the Ga and P species and a comprehensive evaluation of the methodology. The reaction channels described here encompass uni- and bimolecular reactions. As pointed out in the Introduction, unimolecular reactions are assumed to occur more likely than higher order reactions in a low-pressure atmosphere. Calculations of homolytical bond cleavage reactions (*e.g.* symmetric dissociation of

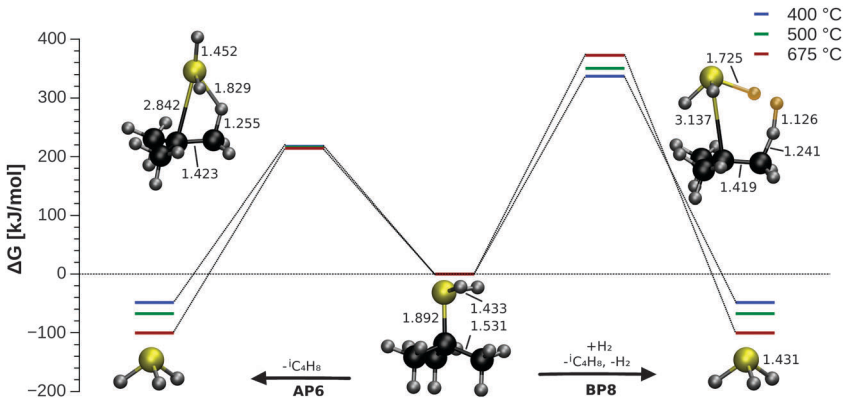

Fig. 7 Decomposition of TBP *via* β-hydrogen elimination of isobutene (reaction to the left) and bimolecular concerted elimination of isobutene and H_2 (reaction to the right) leading to phosphine, respectively. Changes in Gibbs energy (ΔG) and barriers (in kJ mol^{-1}) at experimental temperatures. Distances are given in Å.

H_2, cleavage of $H^\bullet$, $CH_3^\bullet$, and $C_2H_5^\bullet$ from TEG) show that this decomposition class is consistently endergonic (for saturated reactants) and can therefore be neglected. Instead, β-hydride elimination reactions seem to be the dominant channel for TEG.

Additionally, some classes of bimolecular reactions have to be considered. These are reactions with the carrier gas H_2 which are thermodynamically accessible.[53] But also the radicals $H^\bullet$, $C_2H_5^\bullet$, t-$C_4H_9^\bullet$, *etc.* might be available in small concentrations as they can be produced in the course of a MOVPE procedure. Especially interesting is the formation of atomic hydrogen which can potentially be thermally desorbed from the substrate at 480–580 °C[16] as well as hydrogen (or carbon hydrates) *via* recombinative desorption.[59] As this work focused on pure gas phase reactions, the investigation of the latter reactions only becomes important when the surface is explicitly considered in the next phase of this study. Heterolytic dissociation reactions leading to ionic species are not considered as those will not occur in the gas phase and are of minor importance when focusing on relevant decomposition products. For example, an alternative (“barrierless”) mechanism for reaction AP6 involving an unstable, ionized intermediate step was proposed for the As-precursor TBA,[15] but the mechanism is probably surface-mediated. It becomes clear that the conclusions about viability of a reaction mechanism cannot be drawn from the thermodynamic data alone. Reaction barriers were calculated only for those exergonic reactions that were likely to occur based on the above assumptions. AP6, for instance, is strongly exergonic but exhibits a large barrier which will result in a very low reaction rate at all but the highest temperatures. Generally, transition state theory is valid here as large molecules and high temperatures are considered.[48]

The distribution of particles and temperature in the chamber are fluctuating irregularly. The Si-wafer is locally heated, so the highest temperature region is at and directly above the surface. The carrier gas flow induces a flux that transports the heated gas away from the wafer towards the gas outlet. As a consequence, the temperatures applied in this study (experimental surface temperatures of 400, 500 and 675 °C) represent upper bounds for the temperature in the gas phase. This has consequences in interpreting the calculated energies: since the change in Gibbs energy becomes more negative (or less positive) with an increase in temperature for all elementary reactions, a higher temperature means a more exergonic reaction. Thus, the presented thermodynamic values represent a lower bound for the discussed MOVPE precursors. In the real system, the reaction enthalpies will be less favorable due to colder local temperatures further away from the surface. The situation is different for the reaction barriers: as the barrier of a reaction generally *increases* with an increase in temperature (except AG20 and AP6), the calculated data are upper bounds for the barriers. In the real system, lower temperatures will result in smaller barriers. However, as the temperature dependence of Gibbs energy barriers is not strong, this effect will not be decisive. More important will be the higher kinetic energy of the molecules to overcome these (slightly raised) barriers at higher temperature.

Decomposition reactions on the surface have entirely different mechanisms and may lead to different inert and reactive intermediates. Catalytic effects of the surface might change the relevant barriers drastically, hence studies in this field have to be taken into account.[16,60] Thus we will continue our work in this field by applying periodic calculations to the GaP–Si system within the methodology validated here.

5. Conclusions

In this study, we present a comprehensive reaction catalogue for the gas phase decomposition reactions of triethylgallane ($Ga(C_2H_5)_3$, TEG) and *tert*-butylphosphine ($PH_2(t$-$C_4H_9)$, TBP) with thermodynamic and reaction barrier data based on DFT and *ab initio* (MP2, CCSD(T)) energies. From these data, conclusions can be drawn for the gas phase species relevant for the MOVPE growth of III/V-semiconductor GaP on silicon substrates. For TEG, we find a series of β-hydride elimination reactions as the most probable pathway leading to GaH_3 or even GaH at elevated temperatures (675 °C). Radical cleavage and other reactions as often proposed earlier are found to

exhibit unfavorable thermodynamic characteristics. For TBP, a group 15 analogue of the β-hydride elimination reaction is found to be the energetically most accessible reaction. For all uni- and bimolecular TBP decomposition reactions, the computed barriers are very high leading to the conclusion of mainly the original precursor arriving at the surface. Methodologically, we could show that dispersion-corrected DFT computations at the PBE-D3 level perform well in comparison to MP2 and CCSD(T) benchmark data and can be used for further studies of these systems.

Acknowledgements

We thank Prof. Kerstin Volz, Prof. Wolfgang Stolz and Dr. Andreas Beyer (Marburg) for fruitful discussions and insights into experimental details. Funding by the DFG through the Research Training Group ''Functionalization of Semiconductors'' (GRK 1782) is gratefully acknowledged. A.S. thanks the Beilstein Institut, Frankfurt am Main, for generous support *via* a PhD fellowship. Computational resources were kindly provided by HRZ Marburg, LOEWE-CSC Frankfurt and HLR Stuttgart.

References

1 (*a*) B. Kunert, K. Volz, I. Németh and W. Stolz, *J. Lumin.*, 2006, **121**, 361; (*b*) N. Koukourakis, C. Buckers, D. A. Funke, N. C. Gerhardt, S. Liebich, S. Chatterjee, C. Lange, M. Zimprich, K. Volz, W. Stolz, B. Kunert, S. W. Koch and M. R. Hofmann, *Appl. Phys. Lett.*, 2012, **100**, 092107; (*c*) B. Kunert, K. Volz, J. Koch and W. Stolz, *Appl. Phys. Lett.*, 2006, **88**, 182108; (*d*) S. Liebich, M. Zimprich, A. Beyer, C. Lange, D. J. Franzbach, S. Chatterjee, N. Hossain, S. J. Sweeney, K. Volz, B. Kunert and W. Stolz, *Appl. Phys. Lett.*, 2011, **99**, 071109; (*e*) B. Kunert, K. Volz and W. Stolz, *Phys. Status Solidi B*, 2007, **244**, 2730.
2 D. Liang and J. E. Bowers, *Nat. Photonics*, 2010, **4**, 511.
3 B. Kunert, K. Volz, J. Koch and W. Stolz, *J. Cryst. Growth*, 2007, **298**, 121.
4 A. Beyer, J. Ohlmann, S. Liebich, H. Heim, G. Witte, W. Stolz and K. Volz, *J. Appl. Phys.*, 2012, **111**, 83534.
5 A. Beyer, I. Németh, S. Liebich, J. Ohlmann, W. Stolz and K. Volz, *J. Appl. Phys.*, 2011, **109**, 083529.
6 P. Gibart, *Rep. Prog. Phys.*, 2004, **67**, 667.
7 C. Wang, *J. Cryst. Growth*, 2004, **272**, 664.
8 M. Jacko and S. J. W. Price, *Can. J. Chem.*, 1963, **41**, 1560.
9 A. Brauers, *Prog. Cryst. Growth Charact. Mater.*, 1991, **22**, 1.
10 M. Trachtman and S. Beebe, *J. Phys. Chem.*, 1995, 15028.
11 D. Moscatelli, P. Caccioppoli and C. Cavallotti, *Appl. Phys. Lett.*, 2005, **86**, 91106.
12 R. Schmid and D. Basting, *J. Phys. Chem. A*, 2005, **109**, 2623.
13 J. Lee, Y. Kim and T. Anderson, *ECS Trans.*, 2009, **25**, 41.
14 T. R. Gow and R. Lin, *J. Cryst. Growth*, 1990, **106**, 577.
15 M. Boero, Y. Morikawa, K. Terakura and M. Ozeki, *J. Chem. Phys.*, 2000, **112**, 9549.
16 N. Bahlawane, F. Reilmann, L.-C. Salameh and K. Kohse-Höinghaus, *J. Am. Soc. Mass Spectrom.*, 2008, **19**, 947.
17 A. Saxler, D. Walker, P. Kung, X. Zhang, M. Razeghi, J. Solomon, W. C. Mitchel and H. R. Vydyanath, *Appl. Phys. Lett.*, 1997, **71**, 3272.
18 B. Wolbank and R. Schmid, *Chem. Vap. Deposition*, 2003, **9**, 272.
19 (*a*) S. H. Li, C. A. Larsen, N. I. Buchan and G. B. Stringfellow, *J. Electron. Mater.*, 1989, **18**, 457; (*b*) Y. S. Hiraoka, M. Mashita, T. Tada and R. Yoshimura, *Appl. Surf. Sci.*, 1992, **60–1**, 246; (*c*) C. H. Chen, D. S. Cao and G. B. Stringfellow, *J. Electron. Mater.*, 1988, **17**, 67.
20 K. Volz, A. Beyer, W. Witte, J. Ohlmann, I. Németh, B. Kunert and W. Stolz, *J. Cryst. Growth*, 2011, **315**, 37.
21 A. Y. Timoshkin, *Coord. Chem. Rev.*, 2005, **249**, 2094.
22 A. Y. Timoshkin and H. F. Schaefer III, *J. Phys. Chem. C*, 2008, **112**, 13816.
23 A. Y. Timoshkin, H. F. Bettinger and H. F. Schaefer III, *J. Cryst. Growth*, 2001, **222**, 170.
24 B. Mondal, D. Mandal, D. Ghosh and A. K. Das, *J. Phys. Chem. A*, 2010, **114**, 5016.
25 J. Schäfer, A. Simons, J. Wolfrum and R. A. Fischer, *Chem. Phys. Lett.*, 2000, **319**, 477.
26 A. Szabó, A. Kovács and G. Frenking, *Z. Anorg. Allg. Chem.*, 2005, **631**, 1803.
27 A. Y. Timoshkin and G. Frenking, *J. Am. Chem. Soc.*, 2002, **124**, 7240.
28 G. Zimmermann, A. Ougazzaden and A. Gloukhian, *Mater. Sci. Eng., B*, 1997, **44**, 37.
29 S. J. Hashemifar, P. Kratzer and M. Scheffler, *Phys. Rev. B: Condens. Matter Mater. Phys.*, 2010, **82**, 214417.
30 M. J. Frisch, G. W. Trucks, H. B. Schlegel, G. E. Scuseria, M. A. Robb, J. R. Cheeseman, G. Scalmani, V. Barone, B. Mennucci, G. A. Petersson, H. Nakatsuji, M. Caricato, X. Li, H. P. Hratchian, A. F. Izmaylov, J. Bloino, G. Zheng, J. L. H. Sonnenberg, M. Ehara, K. Toyota, R. Fukuda, J. Hasegawa, M. Ishida, T. Nakajima, Y. Honda, O. Kitao, H. Nakai, T. Vreven, J. A. Montgomery Jr., J. E. Peralta, F. Ogliaro, M. Bearpark, J. J. Heyd, E. Brothers, K. N. Kudin, V. N. Staroverov, R. Kobayashi, J. Normand, K. Raghavachari, A. Rendell, J. C. Burant, S. S. Iyengar, J. Tomasi, M. Cossi, N. Rega, N. J. Millam, M. Klene, J. E. Knox, J. B. Cross, V. Bakken, C. Adamo, J. Jaramillo, R. Gomperts, R. E. Stratmann, O. Yazyev, A. J. Austin, R. Cammi, C. Pomelli, J. W. Ochterski, R. L. Martin, K. Morokuma, V. G. Zakrzewski, G. A. Voth, P. Salvador, J. J. Dannenberg, S. Dapprich, A. D. Daniels, Ö. Farkas, J. B. Foresman, J. V. Ortiz, J. Cioslowski and D. J. Fox, *Gaussian 09, Rev. C.01*, Gaussian, Inc., Wallingford CT, 2009.
31 TURBOMOLE V6.3, a development of University of Karlsruhe and Forschungszentrum Karlsruhe GmbH, 1989–2007, TURBOMOLE GmbH, since 2007; available from www.turbomole.com, **2012**.
32 R. Ahlrichs, M. Bär, M. Häser, H. Horn and C. Kölmel, *Chem. Phys. Lett.*, 1989, **162**, 165.

33 J. P. Perdew, K. Burke and M. Ernzerhof, *Phys. Rev. Lett.*, 1996, **77**, 3865.
34 S. Grimme, J. Antony, S. Ehrlich and H. Krieg, *J. Chem. Phys.*, 2010, **132**, 154104.
35 S. Grimme, S. Ehrlich and L. Goerigk, *J. Comput. Chem.*, 2011, **32**, 1456.
36 O. Christiansen, H. Koch and P. Jørgensen, *Chem. Phys. Lett.*, 1995, **243**, 409.
37 C. Hättig and F. Weigend, *J. Chem. Phys.*, 2000, **113**, 5154.
38 F. Weigend, M. Häser, H. Patzelt and R. Ahlrichs, *Chem. Phys. Lett.*, 1998, **294**, 143.
39 C. Hättig, A. Hellweg and A. Köhn, *Phys. Chem. Chem. Phys.*, 2006, **8**, 1159.
40 P. Deglmann and F. Furche, *J. Chem. Phys.*, 2002, **117**, 9535.
41 P. Deglmann, F. Furche and R. Ahlrichs, *Chem. Phys. Lett.*, 2002, **362**, 511.
42 M. Tafipolsky and R. Schmid, *J. Comput. Chem.*, 2005, **26**, 1579.
43 O. Sackur, *Ann. Phys.*, 1911, **36**, 958.
44 K. Eichkorn, O. Treutler, H. Ohm, M. Häser and R. Ahlrichs, *Chem. Phys. Lett.*, 1995, **242**, 652.
45 F. Weigend, *Phys. Chem. Chem. Phys.*, 2006, **8**, 1057.
46 F. Weigend and R. Ahlrichs, *Phys. Chem. Chem. Phys.*, 2005, **7**, 3297.
47 B. C. Hoffman, C. D. Sherrill and H. F. Schaefer III, *J. Mol. Struct.*, 1996, **370**, 93.
48 H. Simka, B. G. Willis and I. Lengyel, *Prog. Cryst. Growth Charact. Mater.*, 1997, **35**, 117.
49 N. W. Mitzel, C. Lustig, R. J. F. Berger and N. Runeberg, *Angew. Chem., Int. Ed.*, 2002, **41**, 2519.
50 J. R. Durig, *J. Mol. Struct.*, 1977, **30**, 77.
51 (*a*) H. Oberhammer, R. Schmutzler and O. Stelzer, *Inorg. Chem.*, 1978, **17**, 1254; (*b*) J. Bruckmann and C. Krüger, *Acta Crystallogr., Sect. C: Cryst. Struct. Commun.*, 1995, **51**, 1152.
52 L. Bartell and H. Burgi, *J. Am. Chem. Soc.*, 1972, **531**, 5239.
53 Test calculations with different partial pressures for the carrier gas H_2 (5×10^{-2} atm) and the precursor molecules (5×10^{-4} atm) (for application of this approach, see E. Kalered, H. Pedersen, E. Janzén and L. Ojamäe, *Theor. Chem. Acc.*, 2013, **132**, 1) resulted in a constant shift of all reactions containing H_2 as a reactant or product. None of the conclusions regarding endo- or exothermicity of the reactions is affected by this shift.
54 D. R. B. Brittain, C. Y. Lin, A. T. B. Gilbert, E. I. Izgorodina, P. M. W. Gill and M. L. Coote, *Phys. Chem. Chem. Phys.*, 2009, **11**, 1138.
55 W. Koch and M. C. Holthausen, *A Chemist's Guide to Density Functional Theory*, Wiley-VCH, Weinheim, New York, 2nd edn, 2001.
56 G. H. Fan, R. D. Hoare, M. E. Pemble, I. M. Povey, A. G. Taylor and J. O. Williams, *J. Cryst. Growth*, 1992, **124**, 49.
57 (*a*) D. S. Matteson, *Organometallic Reaction Mechanisms*, Academic Press, New York and London, 1974, ch. 5; (*b*) J. E. Huheey, E. A. Keiter and R. L. Keiter, *Inorganic Chemistry, Principles of Structure and Reactivity*, Harber Collins College Publishers, 1993, 4th edn, p. 699.
58 A. Stegmüller and R. Tonner, in preparation.
59 C. Schwalb, M. Dürr and U. Höfer, *Phys. Rev. B: Condens. Matter Mater. Phys.*, 2009, **80**, 085317.
60 S. Salim, C. K. Lim and K. F. Jensen, *Chem. Mater.*, 1995, **7**, 507.